

Review

# Steroid-Based Liquid Crystalline Polymers: Responsive and Biocompatible Materials of the Future

Bartłomiej Czubak<sup>1</sup>, Nicholas J. Warren<sup>2</sup> and Mamatha Nagaraj<sup>1,\*</sup><sup>1</sup> School of Physics and Astronomy, University of Leeds, Leeds LS2 9JT, UK; pybcz@leeds.ac.uk<sup>2</sup> School of Chemical and Process Engineering, University of Leeds, Leeds LS2 9JT, UK; n.warren@leeds.ac.uk

\* Correspondence: M.Nagaraj@leeds.ac.uk; Tel.: +44-(0)-113-343-8475

**Abstract:** Steroid-based liquid crystal polymers and co-polymers have come a long way, with new and significant advances being made every year. This paper reviews some of the recent key developments in steroid-based liquid crystal polymers and co-polymers. It covers the structure–property relationship between cholesterol and sterol-based compounds and their corresponding polymers, and the influence of chemical structure and synthesis conditions on the liquid crystalline behaviour. An overview of the nature of self-assembly of these materials in solvents and through polymerisation is given. The role of liquid crystalline properties in the applications of these materials, in the creation of nano-objects, drug delivery and biomedicine and photonic and electronic devices, is discussed.

**Keywords:** liquid crystal; polymer; cholesterol; block copolymer; self-assembly; polymerisation-induced self-assembly



**Citation:** Czubak, B.; Warren, N.J.; Nagaraj, M. Steroid-Based Liquid Crystalline Polymers: Responsive and Biocompatible Materials of the Future. *Crystals* **2022**, *12*, 1000. <https://doi.org/10.3390/cryst12071000>

Academic Editor: Ingo Dierking

Received: 1 June 2022

Accepted: 12 July 2022

Published: 19 July 2022

**Publisher's Note:** MDPI stays neutral with regard to jurisdictional claims in published maps and institutional affiliations.



**Copyright:** © 2022 by the authors. Licensee MDPI, Basel, Switzerland. This article is an open access article distributed under the terms and conditions of the Creative Commons Attribution (CC BY) license (<https://creativecommons.org/licenses/by/4.0/>).

## 1. Introduction

In 1888, botanist Friedrich Reinitzer observed an unexpected double melting point in a crystal, cholesteryl benzoate, collected from the root of a carrot [1]. The material, cholesteryl benzoate, was the first liquid crystal and its discovery marks the start of the modern liquid crystal research. Over the last century, liquid crystals (LCs) have contributed to some of the greatest technological leaps, such as flat-screen televisions, mobile phones and sensors [2–9]. Whilst cholesterol by itself is not liquid crystalline, a number of its derivatives are; most notably, esters of cholesterol [10–14]. These compounds, due to the inherent chiral nature of sterols, form a chiral nematic (N\*) phase. Cholesterol plays an important role within biological systems. It is an essential component of all animal cells. It controls the permeability of the cell membrane and plays a key part in the formation of lipid rafts [15].

Liquid crystal polymers are higher-molecular-weight liquid crystals that exhibit mesomorphic behaviour. They have been extensively investigated for their fundamental properties and as thermoplastics, photochromic, semiconducting, etc., materials [16–21]. Even though the N\* phase observed back in 1888 was in low-molecular-weight liquid crystals (LMWLC), it was hypothesised that this phase could be observed in polymers or other higher-molecular weight liquid crystals (HMWLCs). Early work on liquid crystalline polymers forming the N\* phase was performed with cholesterol and its derivatives [22]. The resulting polymers, however, did not form the N\* phase, unlike their corresponding monomers; instead, they formed higher ordered smectic phases [23,24]. In 1978, Finkelmann et al., prepared the first enantiotropic cholesteric polymer by polymerising mixtures of cholesterol-based monomers with short and long spacers [25]. Expanding on their earlier work on liquid crystalline polymer synthesis, Finkelmann then proceeded to develop a polymer series with an N\* phase, moving on to describe the first polymer with a biaxial N\* phase [26]. The key step in this process was decoupling the motion of the polymer backbone from the mesogenic group via a ‘spacer’ group between the two.

There is a wide arsenal of synthetic approaches for the preparation of monomers based on cholesterol and other steroids (Figure 1). However, the liquid crystalline order in their corresponding polymers is highly influenced by the properties of the polymer, such as its molar mass dispersity, degree of polymerisation and, in the case of block copolymers (Figure 1A), the weight ratio of each of the blocks. Work by Shibaev in 1979 showed an ambiguous phase formation in methacrylic copolymers bearing cholesterol and butylmethacrylate [27]. While they displayed textures and a selective reflection similar to those observed in an  $N^*$  phase in LMWLCs in bulk, these textures were not observed in thin films. In thin film they instead showed textures similar to those of standard smectics. Another example of a polymer forming higher-order structures compared to the corresponding monomers was observed by Xu et al. [28]. They found that the  $N^*$  phase was only observed in monomers, but not in polymers bearing the same mesogen. The polymers instead formed a smectic A (SmA) phase due to the limited flexibility of the backbone and spacer units hindering the formation of the helix of the  $N^*$  phase.

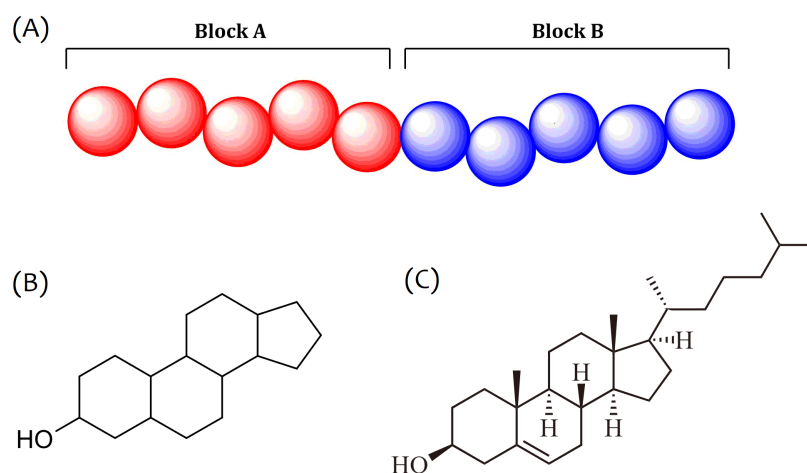


**Figure 1.** (A) Cartoon representation of a block copolymer. The repeating units are bound together by a covalent bond resulting in an amphiphilic molecule. (B) Chemical structure of generic sterol and (C) cholesterol.

## 2. Liquid Crystalline Polymers Bearing Sterol Side Groups

### *Synthesis and Structure–Property Relationships*

Homopolymers bearing side-chain cholesteryl mesogens tend to form smectic phases (predominantly SmA) over a wide range of temperatures, with only a selected few showing both chiral nematic and smectic phases [29]. This is due to the choice of the chemical structures of the spacer groups and backbone. As the cholesteryl molecule is intrinsically chiral, it only forms chiral phases in polymers when the mesogen is free to do so. Initial preparation of the homopolymers bearing side-chain cholesteryl mesogens was achieved using free radical polymerisation. However, this led to the poor dispersity of the polymer, which hindered the formation of the mesophases. Nowadays, reversible-deactivation radical polymerisation (RDRP) reactions are employed, which offer a much more sophisticated approach to the preparation of the polymers. Methods such as reversible addition-fragmentation chain-transfer polymerisation (RAFT) [30,31] and atom transfer radical polymerisation (ATRP) [32,33] are commonly used as they offer tighter control over the degree of polymerisation and narrow polydispersity over the resulting polymer.

The nature and, hence, the influence of the flexible spacer on the polymers is a key parameter that controls the phases and transition temperatures. It does so by decoupling the mesogenic units and allowing them to freely form the mesophases. Both the type of the spacer and the length of the spacer are important [34]. Additionally, the stability

and formation of the N\* phase in polymers can be affected even by a small change in the chemical structure of the polymer.

Finkelmann et al. also prepared an enantiotropic liquid crystalline polymer with an N\* phase by mixing different equal parts monomers with short spacers and longer spacers based on alkylbenzene ester [35]. Whilst this was not a homopolymer, it paved the way for a better understanding of the influence of the spacer group on the resulting mesophases. The influence of the spacer on the properties of the polymer was further demonstrated by Hu et al. [36], where they showed that longer spacer length lead to lower phase transition temperatures and wider LC temperature ranges in polymers bearing cholesteryl side groups. The selective reflection of the polymers was also shown to blue shift as the spacer lengths were increased or the rigidity of the mesogens decreased. This was further explored by Yang et al., who showed that the degree of polymerisation of the polymer does not have a significant effect on the polymers without flexible spacers and with a stiffer methacrylic backbone [37]. However, it does have an effect on the more flexible acrylic backbone where the LC behaviour is observed only upon passing a critical threshold of molecular weight of  $12 \times 10^3 \text{ g mol}^{-1}$ . By switching the spacer from an ether (Figure 2A) to an equivalent ester, (Figure 2B) Yang et al. demonstrated that the transition temperature to the N\* mesophase shifted from  $-27^\circ\text{C}$  in the ether linker to  $72^\circ\text{C}$  in the ester case whilst having little impact on the clearing temperature [34]. This switching of the spacer from an ether to an equivalent ester also caused the polymer to display crystallisation rather than a glass transition. A much more dramatic change was observed when the second ether in the linker was replaced with another ester group (Figure 2C). In this example, the polymer only displayed a monotropic smectic phase and no N\* phase was observed. For the N\* phase to form, the spacer length had to be increased to  $n = 10$ . This arises from the relative stiffness of the C=O bond compared to C-O, which hinders the freedom of the mesogen to order itself. Klok et al. showed that the covalent incorporation of cholesterol moiety to a low-molecular-weight L-lactic acid oligomers resulted in the formation of thermotropic liquid crystal smectic phases [38]. While the mesogen was a small part of the overall molecule, its strong tendency to form the mesophase was expressed in the larger molecule.

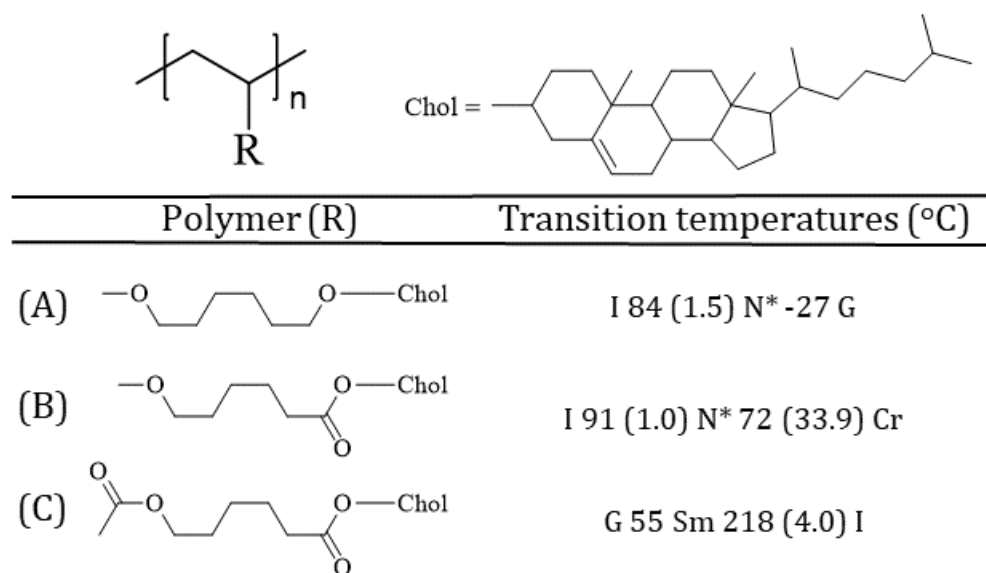


**Figure 2.** An example of the influence of chemical differences in the spacer connecting the backbone and the cholesteryl mesogen, on the liquid crystallinity of the material. The introduction of each of the ester groups (A–C) gradually increases the relative stiffness of the backbone. N\*—chiral nematic, I— isotropic, G—glass, Cr—crystal and Sm—smectic.

A number of studies have been carried out on block-copolymers (BCPs) bearing side-chain cholesteryl mesogens. A BCP bearing a chiral but non-mesogenic menthol group

and a cholesterol mesogen was prepared by Wang et al. [39] The introduction of the non-mesogenic unit resulted in the lowering of the glass transition temperature,  $T_g$  but led to a narrower mesophase temperature range. The corresponding cholesterol homopolymer did not form the  $N^*$  phase, and instead showed a chiral smectic phase. Only upon the addition of chiral menthol, an  $N^*$  phase was observed in the BCPs. This, however, led to a significant decrease in the temperature range at which the mesophase was observed, from 145 °C to 24 °C, resulting in limited applications of this polymer system. The self-assembly behaviour of block copolymers has been a topic of great interest due to their application potential. Therefore, in the next section, the structure–property relationship of BCPs and their synthesis methods are covered while discussing their applications.

### 3. Applications of Sterol-Based Liquid Crystalline Block Copolymers

#### 3.1. Self-Assembly Behaviour: Creation of Micelles and Nano-Objects

Block copolymers (BCPs) are well known to self-assemble in bulk and in solution due to their intrinsic amphiphilic properties. Hamley et al. studied a series of block copolymers based on polystyrene and a methacrylic cholesterol monomer [32]. They reported the formation of a stable SmA phase within all of the polymers with varied LC content. The copolymers were probed using small-angle X-ray scattering (SAXS) where multiple scattering peaks were observed. The smectic A monolayer had a distinct and sharp peak at approx.  $d = 2.1$  nm with a more diffuse peak observed at temperatures below the smectic transition. These lower-intensity peaks corresponded to smectic-like ordering with interdigitating groups where the sample was unable to align as a result of the partial crystallisation of the material. Venkataraman et al. prepared a series of disk-like micelles and stacked columns of the micelles from mPEG<sub>113</sub>-b-P(MTC-Chol)<sub>11</sub> block copolymer [40]. Figure 3 shows the transmission electron microscopy (TEM) images of aqueous self-assembled nanostructures formed by mPEG<sub>113</sub>-b-P(MTC-Chol)<sub>11</sub>. It shows the various orientations of the stacked structures, including face-on, intermediate ellipsoidal, edge-on and stacked-disk. This unique formation of micelles was attributed to the self-association of the cholesterol moieties in smectic order. Depending on the percentage of the LC content, the disks displayed a unique ability to stack perpendicular to the major axis in a process driven by the narrow polydispersity (PD) of the copolymer chains, combined with the liquid crystalline order as a driving force.

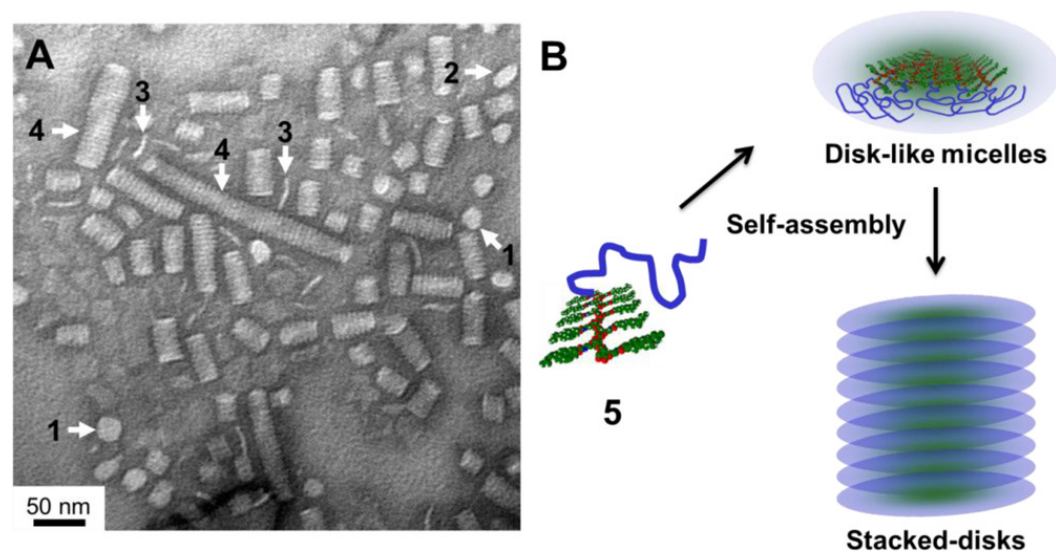


**Figure 3.** (A) TEM micrographs of stained aqueous self-assembled nanostructures formed by mPEG<sub>113</sub>-b-P(MTC-Chol)<sub>11</sub>. Arrows 1–3 show the face-on, intermediate ellipsoidal, and edge-on orientations of the structures, respectively; arrow 4 shows the stacked-disk orientation (B) Schematic representation of the mechanism driving the formation of stacked-disk micelles. Reprinted with permission from Venkataraman et al., *Macromolecules*, **2013**, *46*, 4839–4846 [40].

The morphology of BCP nano-objects as a function of pH was investigated by Guo et al. [41]. for a diosgenyl functionalised block copolymer, mPEG<sub>43</sub>-PMCC<sub>25</sub>-P(MCC-DHO)<sub>1</sub>. Under basic pH conditions, the polymer formed nanospheres. However, a transition to nanofibres was facilitated by acidifying the solution (Figure 4). This transition was due to the ionization of the carboxylic groups, which subsequently repelled each other to promote an increase in the preferred curvature of the interface. Interestingly, the size of the nanospheres was directly correlated with the pH. Particles prepared at pH = 2 had a radius of 324 nm and those prepared at pH = 6 had a radius of 232 nm.

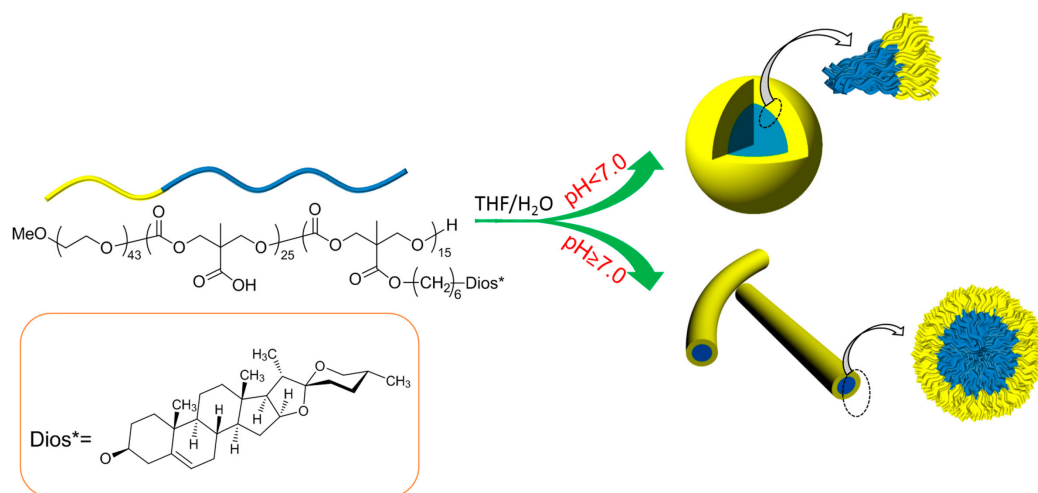


**Figure 4.** Self-assembly behaviour of mPEG<sub>43</sub>-PMCC<sub>25</sub>-P(MCC-DHO)<sub>1</sub> as a function of pH in tetrahydrofuran/water. Reprinted with permission from Guo et al., *Nanomaterials*, 2017, 7, 169 [41].

A comprehensive study on the self-assembly of a cholesterol-functionalised liquid crystalline block copolymer of poly(cholesteryl methacryloyloxy ethyl carbonate)-b-(poly(ethylene glycol)methyl ether methacrylate), (PChEMA<sub>m</sub>-b-POEGMA<sub>n</sub>), in different solvents was carried out by Li et al. [42]. By controlling the weight fraction of the LC block, a series of structures was observed (Figure 5). The two factors that dictated the self-assembly, the smectic order within the LC block and the amphiphilic nature of the copolymer were expressed differently depending on the solvent. The LC order was found to be absent in a tetrahydrofuran(THF)/water system, which indicates that the amphiphilicity plays an important role in the self-assembly process. In the 1,4-dioxane/water system, a smectic order was observed within micelles, indicating that the LC order plays a more important role in the growth and morphology of the micelles. This change in behaviour was explained by the difference in the affinity between the cholesteryl block and the solvents. The Flory–Huggins interaction parameter (*X*) between the PChol and THF is 0.63, whereas between PChol and dioxane it is 0.92. This implies that THF is a much better solvent for the polymer, which results in a reduced driving force for self-assembly and an absence of LC order. A transition between smectic nanofibers and smectic ellipsoidal vesicles was observed for a cholesteryl-containing polymer with a biodegradable poly(trimethylene carbonate) backbone (Figure 5). These structures assembled into rods under dioxane, but reoriented from lamellar to ellipsoidal vesicles upon the addition of water.

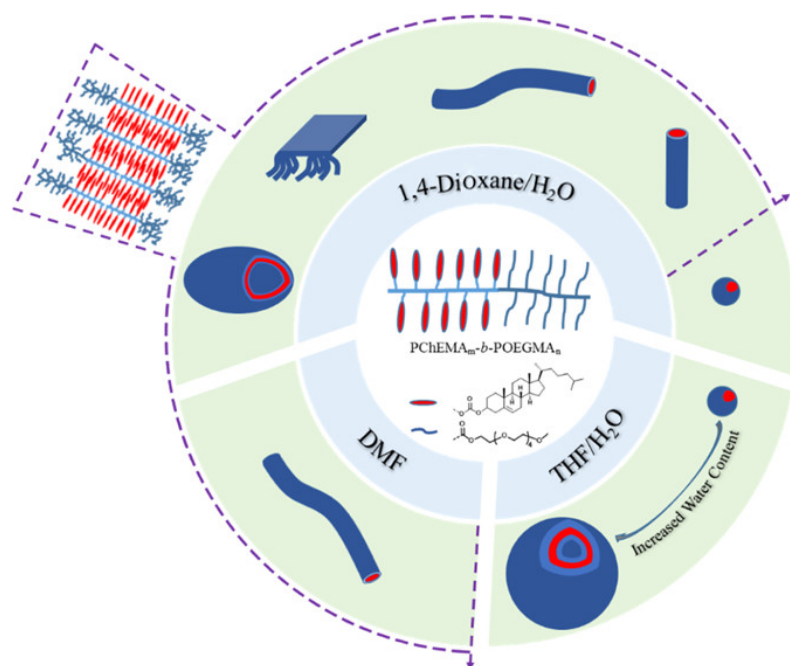


**Figure 5.** The adaptable nature of the cholesterol-bearing diblock BCP allows it to self-assemble into a plethora of structures in different solvents and concentrations. Reprinted with permission from Li et al., *Langmuir*, 2018, 34, 11034–11041 [42].

Krishnasam et al. investigated the reversible inversion of chirality in block copolymers of poly(methyl methacrylate) and poly(cholesteryloxyhexyl methacrylate) [43]. Chirality switching is potentially a useful method for the application of block copolymer in novel electronic and photonic materials, especially when it happens in response to a thermal change [44–46]. This system of copolymers of poly(methyl methacrylate) and poly(cholesteryloxyhexyl methacrylate) was the first reported system capable of switching chirality without chiral dopants, making it additive-free. The inversion of chirality was also observed in polymers bearing shorter poly(cholesteryloxyhexyl methacrylate) (PChMA) chains, which possess syndiotacticity (repeating units have alternating stereochemical configurations). The combination seems to lead to tightly packed side chains where the inversion of chirality overcomes the energy penalty at lower temperature. Figure 6 shows the inversion of chirality observed in PChMA-*b*-PMMA BCP. The graphs show the plot of ellipticity measured as a function of wavelength in chiral SmA and SmC phases, measured through circular dichroic (CD) spectroscopy.

The self-assembly behaviour in aqueous solutions of a cholesterol-bearing block copolymer PP<sub>2</sub>-*g*-LC<sub>4</sub> with a flexible hydrophobic backbone was studied by Yang et al. [47]. The BCP consisted of poly(ethylene oxide) block and a mesogenic cholesteryl pendant group. One of the structures observed was a hollow concentric spherical vesicle with SmA order in the shells. These structures exhibited an interdigitating smectic A phase, with LC mesogens grafted onto a backbone of poly-(ethylene oxide)-block-polybutadiene via the “thiol-ene” radical addition reaction. This also marks the first time a spherical arrangement was observed for copolymers comprising a polybutadiene backbone and an LC group. Previously, ellipsoidal or faceted structures were observed [48,49].

A biodegradable BCP bearing cholesteryl mesogen was prepared by Zhou et al. via ring-opening polymerisation [50]. After solvent switching from dioxane to water, nanofibres were obtained (Figure 7). The vesicular wall possessed a smectic order, leading to uniform wall thickness. The nanofibres then, upon contact with each other, formed lamellae that further transformed into ellipsoidal vesicles.

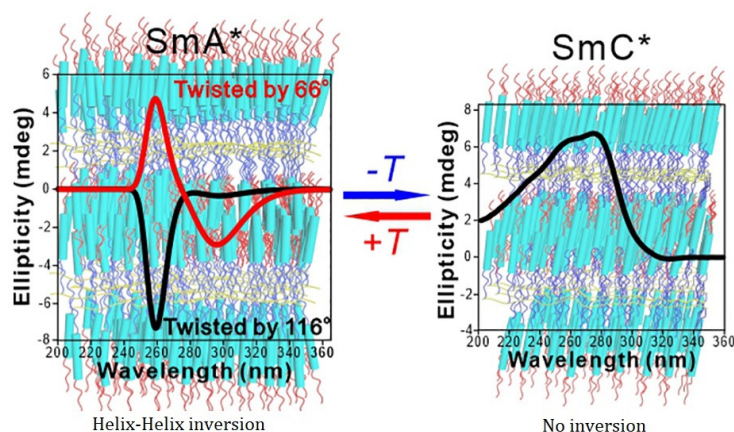


**Figure 6.** Inversion of chirality observed in PChMA-b-PMMA BCP measured through circular dichroism (CD) experiments. The graphs show the plots of ellipticity, measured as a function of wavelength in chiral SmA and SmC phases. The blue rods represent the LC mesogens arranged in layer structures. T represents the temperature. Reprinted with permission from Krishnasamy et al., *Macromolecules*, 2020, 53, 4193–4203 [43].

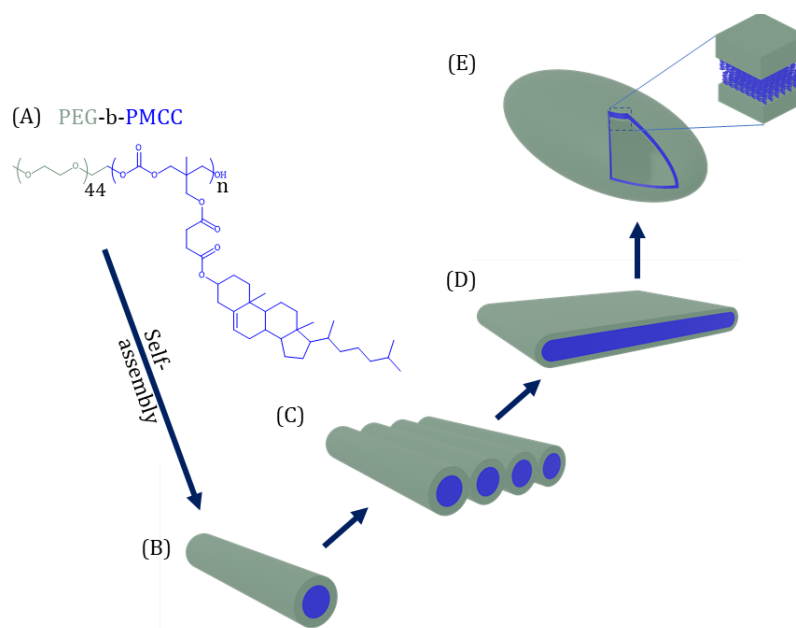


**Figure 7.** The morphological evolution of self-assembled nanostructures observed for PEG-b-PMCC BCP. (A) Chemical structure of PEG-b-PMCC BCP. The schematic representation of (B) the initial nanofibers formed, (C) the fusion of nanofibers, (D) the formation of lamella structure from fused nanofibers and (E) the rearrangement of lamellar structures into ellipsoidal vesicles with LC order within the membrane.

A unique morphology of self-assembled nanostructures was reported by Jia et al. [51]. Nanoribbons bearing smectic stripes were formed upon nanoprecipitation into dioxane (Figure 8). These ribbons were flexible enough to form small creases. Increasing the initial concentration of the BCP during the nanoprecipitation lead to the formation of wider ribbons with more folds. Figure 8 shows TEM images of these nanoribbons for different polymer concentrations.

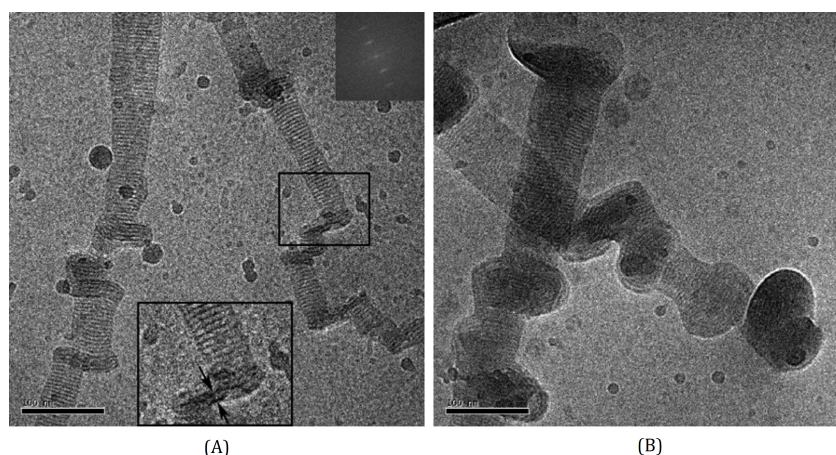


**Figure 8.** Nanoribbons formed by PEG<sub>45</sub>-b-PCpEChol<sub>3</sub>. (A) Starting polymer concentration = 0.1 wt%; (B) starting concentration = 0.5 wt%. Note that the smectic stripes formed at the sides of the ribbons. Reprinted with permission from Jia et al., *Langmuir*, **2012**, *28*, 11215–11224 [51].

A metal-mediated self-assembly of hydrophilic BCPs was developed as a method for the facile preparation of organic–inorganic hybrid nanomaterials under aqueous conditions. Jeong et al. demonstrated that the liquid crystalline order that a cholesterol mesogen contributes to a chelating double-hydrophilic BCP offers a way of controlling chelating sites in nanoparticles [52]. This was a novel method for creating the density modulation of nanoparticles which can be exploited for controlled drug delivery applications.

Jia et al. studied the self-assembly of a PEG-PACHol diblock BCP system in THF/water and obtained monodisperse spherical aggregates with no obvious features [53]. However, the same BCP in a dioxane/water system formed higher-ordered structures, where the smectic order of the cholesterol block was characterised by a striped pattern observed in TEM images (Figure 9). Due to the highly hydrophobic nature of cholesterol mesogen, the self-assembly of BCPs bearing it did not tend to result in complex structures, instead forming spherical structures. On the contrary, the reduced polarity of dioxane/water mixtures had a tendency to plasticise the particle core, providing enhanced mobility to facilitate reorganisation into more complex structures, including ellipsoids and nanocylinders.

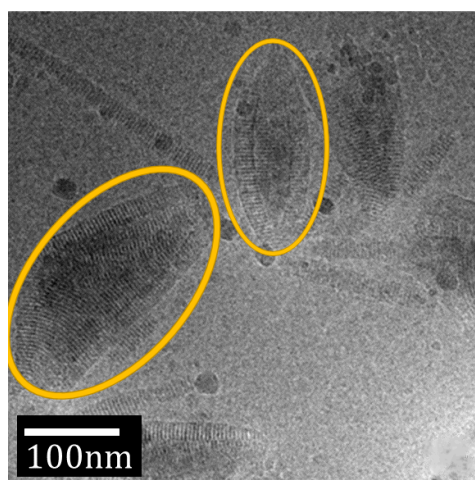


**Figure 9.** Self-assembled structures of PEG<sub>114</sub>-b-PACHol<sub>60</sub> prepared in dioxane/water (14:86) showing the notable smectic stripes decorated on nanocylinders and ellipsoids (circled). Reprinted with permission from Jia et al., *Polymer*, **2011**, *52*, 2565–2575 [53].

Boisse et al. [30] showed different possible structures formed by a cholesterol-bearing amphiphilic BCP with a poly(N,N-diethylacrylamide) hydrophilic block. The polymers

predominantly formed 1D long fibres (Figure 10A–C). A comparative polymer without LC side groups was shown to instead assemble into vesicles and short cylindrical micelles (Figure 10D), demonstrating the important influence of LC order on the self-assembly of BCPs.

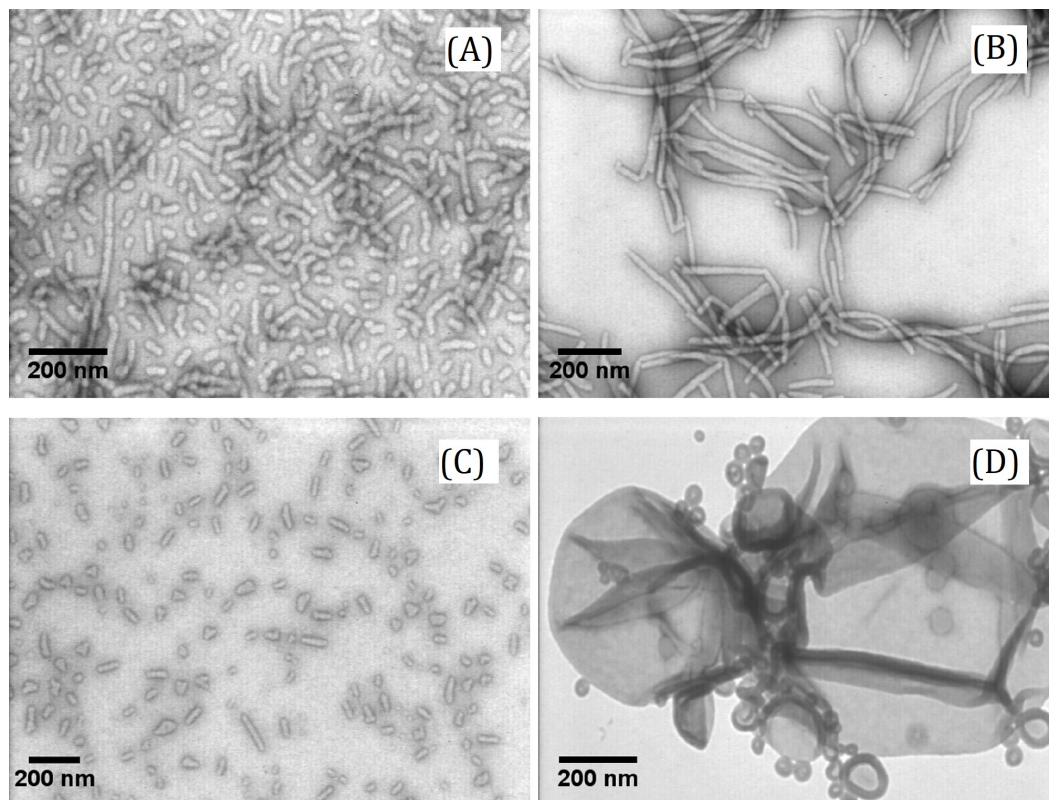


**Figure 10.** TEM micrographs of self-assemblies of (A–C) PMACHol-bPDEAAm at different degrees of polymerisation (DP) of the hydrophilic block. (A) DP = 103, (B) = 30, (C) = 21. (D) PS<sub>136</sub>-b-PDEAAm<sub>32</sub>. Reprinted with permission from Boissé et al., *Macromolecules* 2009, 42, 22, 8688–8696 [30].

### 3.1.1. Polymerisation-Induced Self Assembly

Polymerisation-induced self-assembly (PISA) provides a convenient route for preparing block copolymer nanostructures with high fidelity and tunable functionality. During the PISA process, a soluble precursor polymer is chain extended with a monomer that forms a solvophobic block, resulting in an amphiphilic polymer, which self-assembles to avoid unfavourable interaction with the solvent (Figure 11). It has been widely used to prepare nanoparticles of various morphologies, from simple spherical micelles, worms and vesicles, through to more exotic structures such as ellipsoidal micelles and faceted cuboids. These sorts of structures also frequently exhibit light-, pH- or temperature-responsive transitions between morphologies. While PISA with groups bearing LC mesogens is a relatively under-explored area of research as a whole, it was in fact reported in one of the earliest known PISA papers by Zhang et al. [54], who polymerised CholA monomer ion in the presence of a P(AA-co-PEGA) macromolecular chain transfer agent in an ethanol/water (95:5) solvent to produce poly(acrylic acid-co-poly(ethylene glycol) monomethyl ether acrylate)-b-poly(cholesteryl acryloyloxyethyl carbonate).

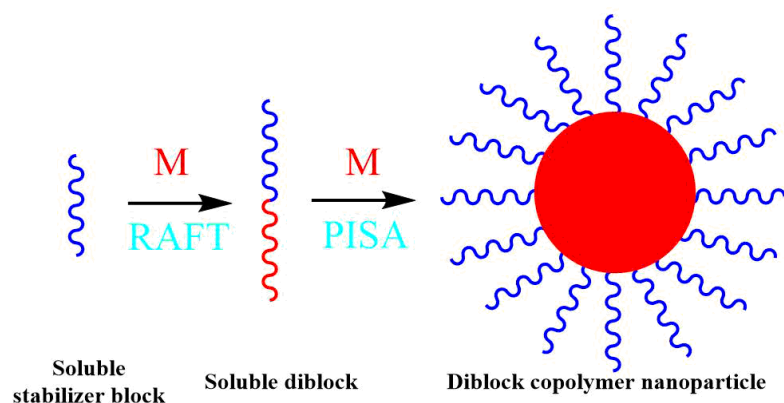


**Figure 11.** Schematic representation of the self-assembly process in polymerisation-induced self-assembly (PISA).

The result was a dispersion of nanocylinders (see Figure 3 in reference [54]) with internal smectic-type order over a broad range of solid concentrations and relative block ratios. The radius of the nanocylinders increased as a function of the chain length of the hydrophobic block. In this case, the LC order was assumed to play a significant role in the assembly formation alongside the traditional driving forces. The study showed that the LC order was preserved and the introduction of it to the system led to the preferential formation of nanofibers over vesicles, observed in an equivalent polystyrene system. An advantage observed upon the introduction of a LC group was the reduction in the polymer dispersity ( $\bar{D}$ ) with higher LC content. While few PISA studies have been performed with steroid-based monomers, the field is starting to gain traction with recent publications focused on the introduction of perfluorinated LC, monomers [55–60], biphenyls [61] and azobenzenes [62–64]. The structures seen within these systems show unique properties such as physical rearrangements upon thermal stimuli. Analogous to systems mentioned earlier, the linker length plays an important role in determining the resulting PISA morphology, with a biphenyl mesogen providing insights into the mechanism underpinning the impact of LC groups within PISA [61]. Longer linkers lead to slower polymerisation kinetics and only the longest ( $C = 11$ ) displayed direct liquid crystalline behaviour with smectic order in the nanorods. The linker also plays a key role in the resulting morphology of the PISA structures. The shortest linker ( $C = 0$ ) formed spheres and sphere aggregates, the intermediate linker ( $C = 6$ ) led to spheres and worms and the longest ( $C = 11$ ) led to the formation of rigid nanorods/nanowires [63].

### 3.1.2. Cholesteryl Polymer-Based Nano-Objects Showing Aggregation-Induced Emission

Triblock BCP bearing a PEG group, a cholesteryl acrylate block and a tetraphenylethene AIEgen (aggregation-induced emission material) side group were synthesised by Zham et al. [65]. The BCP was then self-assembled in a mixture of either dioxane/water or THF/water. Each of the systems self-assembled into a range of nanostructures. The dioxane/water particles formed ellipsoidal vesicles with a constant membrane thickness despite heterogeneity in the overall vesicle diameter. In standard, non-LC PISA systems, the membrane thickness of vesicles is known to be dictated by the solvophobic chain length, where the chains reside in an intermediate state between collapsed globules and fully stretched chains [66,67]. In LC polymers, it has been shown that the membrane formed is a bilayer of fully stretched PACHol groups laying along the normal edge of the membrane. The nanoparticles formed in THF/water were instead spherical and more monodisperse compared to dioxane/water vesicles. The unique combination of LC and AIE properties was probed to see their effect on each other. The LC order arising from the cholesteryl mesogen was undisturbed by either TPE (tetraphenylethylene) or PEG as similar LC behaviour was observed in homopolymers of the cholesteryl acrylate. Both nanospheres and vesicles presented AIE properties with a relatively low quantum yield of 0.74% and 0.76%, respec-

tively. Another triblock BCP bearing tert-Butyl methacrylate (tBA), tetraphenylethylene (TPE) and methacrylic cholesteryl mesogen was studied by Wang et al., [68] in relation to the AIE properties. In this system, the AIE group was introduced to the corona-forming block. While the TPE was still partially dissolved, strong AIE behaviour was observed after micellisation.

### 3.2. Biomedical Applications

Artificial tissue regeneration requires a biocompatible 3D scaffold. The incorporation of liquid crystal order within the scaffold can have the beneficial effect of guiding the direction of cell growth [69]. Particularly, the incorporation of biocompatible components such as cholesterol expands the potential applications for medical devices both in vivo and in vitro. A cholesteryl-bearing BCP has been shown to improve the adhesion and spreading of fibroblast tissue while remaining biocompatible. While the definitive mechanism is not fully understood, the improvement was accredited to the smectic liquid crystal order which helped direct the cells [70]. A triblock BCP was investigated as a potential candidate to use as implant material for cellular scaffolding for dynamic organs such as heart or blood vessels.

A cholesterol-based elastomer was prepared for use in artificial tissue regeneration. The material was made porous by the salt-leaching method in order to promote cell infiltration and promote growth [71]. The SmA order found in the material acted as a template for the pore preparation. These properties made it a suitable candidate for the in vitro growth of neuronal tissue. Xie et al. [72] studied the cytotoxicity of cholesterol-based elastomers. In particular, they focused on the possibility of using the elastomer as a suitable substrate for cell cultures. The results, with glass substrates acting as a control, show that unpolymerised samples are toxic to the cell cultures; however, polymers display high biocompatibility with the cultures. Additionally, due to biocompatibility of the substrate, the cells had better spread and morphology and larger diffusion areas, making these polymers highly suitable for tissue growth and regeneration. Figure 12 shows a representation of the biocompatibility of the cholesterol-based elastomers with the tissue cultures and the resulting tissues samples. The LC content on the surface of the substrate helps the cells adhere, resulting in higher density of pseudopods.

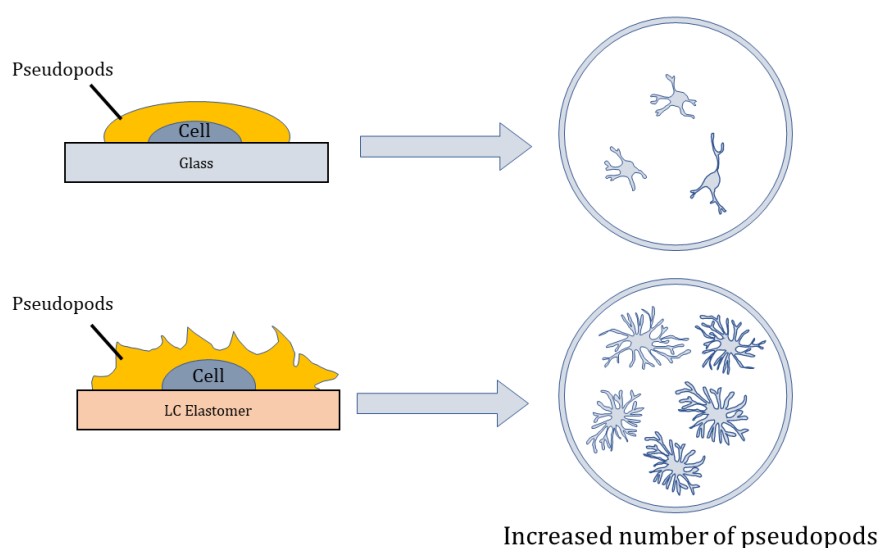


**Figure 12.** An illustration demonstrating the biocompatibility of the cholesterol-based elastomers with the tissue cultures and the resulting tissue samples. The LC content on the surface of the substrate helps the cells adhere, which results in the higher density of pseudopods [72].

A room-temperature smectic elastomer bearing cholesterol mesogen was used for cell culture [73]. The liquid crystalline order rendered the elastomer softer relative to the liquid-crystal-free equivalent elastomer. The porosity, an important factor for cell growth, can be controlled by tuning the amount of cross-linker, and the liquid crystalline properties were controlled by attaching the cholesteryl to either the alpha or gamma position relative to the carboxyl group.

Liu et al. [74] investigated the micelles of copolymer bearing poly(ascrobyl acrylate) and sidechain cholesteryl mesogen for potential applications in the drug delivery of ibuprofen and Nile red dye. Polymers were prepared using RAFT polymerisation followed by desulfurisation and hydrogenolysis. The micelles were then prepared using dialysis over a course of two days. The drug delivery applications were studied as a function of loading the drug molecule and the entrapment efficiency. Nile red was studied as an example of a hydrophobic drug. It was found that having a longer hydrophobic (i.e., cholesterol)-based block helps increase the loading efficiency of the Nile red (Figure 13A) and ibuprofen, as well as increasing the entrapment efficiency of ibuprofen (Figure 13B). The increase in entrapment efficiency was significant (up to 40%) when compared to no polymer at all (5%) and another polymer studied for this application poly(ethylene oxide)-block-poly(lactic acid) (8–9%).

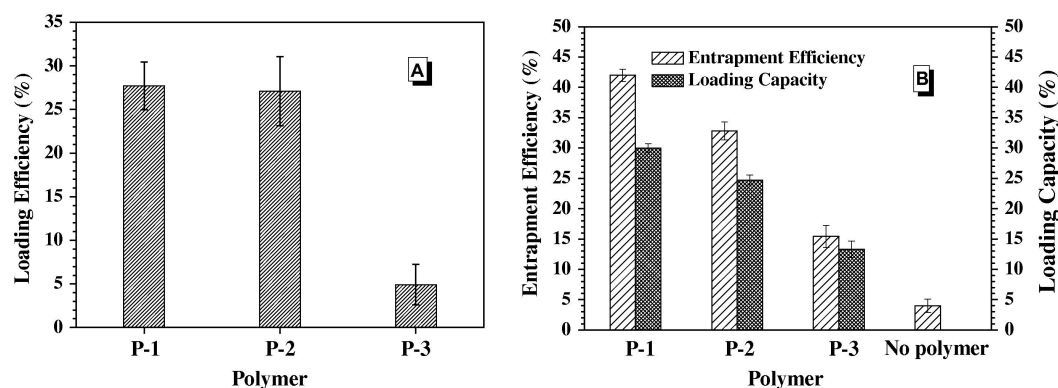


**Figure 13.** (A) Loading efficiency of Nile red. (B) Entrapment efficiency and loading efficiency of ibuprofen poly(lactide-co-glycolide)-cholesterol nanoparticles have also been tested for tumor-targeted delivery of curcumin through intravenous routes, which resulted in low cytotoxicity and high serum stability. P-1, P-2 and P-3 are polymers with gradually decreasing ratios of cholesterol content. Reprinted with permission from Liu et al., *Journal of Colloid and Interface Science*, 2012, 377, 197–206 [74].

A series of BCPs bearing cholesteryl and PEG were prepared via metal-free organocatalytic ring opening polymerisation [75]. These were then self-assembled into micelles and loaded with paclitaxel, an anticancer drug notorious for its difficulty of delivery within aqueous systems. The loaded micelles showed high kinetic stability and demonstrated higher cytotoxicity compared with other delivery methods. Jia et al. [76] reported the development of robust polymersomes capable of controlled cargo release in response to the intercellular reducing environment, which led to the breakage of the disulfide bridge linking the hydrophobic PACHol block and hydrophilic PEG blocks. The system showed good loading capacity and efficiency of calcein, and in vitro studies demonstrated high (up to 80%) drug release upon trigger.

Aliphatic BCPs consisting of PEG blocks and a methacrylic cholesteryl group with a C<sub>6</sub> spacer have been shown to form both smectic A and N\* phases [77]. These polymers also possessed a mesophase range much wider than their corresponding monomers. They also further demonstrated the influence of the spacer on the mesomorphic properties with longer spacers showing wider mesophase range. The mesophase range extended below body temperature, making them suitable for applications in site-specific drug delivery. The incorporation of a cholesterol-bearing sidegroup to a gadolinium-rich amphiphilic carbonate BCP was studied for its influence on the complexation to siRNA (small-interfering nucleic

acid). The cholesteryl group made it insoluble in phosphate-buffered saline (PBS), rendering it impractical to use for siRNA drug delivery [78].

PEG- and cholesterol-based triblock BCPs were prepared via attaching the cholesteryl pendant group to a polymer of fixed length [79]. This led to the formation of SmA phase, spreading to below body temperature. The BCP was then self-assembled by solvent switching into THF/water, leading to the formation of spherical nanoparticles, similar to those described in Section 3.1 above. The nanoparticles were then probed for their potential applications for the targeted delivery of doxorubicin (DOX) for use in vivo. The material displayed acceptable loading content and efficiency. Switching the pH from neutral to low promoted drug release [80].

Another promising BCP bearing cholesterol was studied for applications in the delivery of doxorubicin composed of polynorbornene-cholesterol/PEG [81]. It demonstrated no cytotoxicity by itself, but showed the steady release of DOX at 2% per day in PBS. It had additional positive effects, as it showed decreased cardiac accumulation of DOX compared to free DOX in vivo mice studies.

### 3.3. Photonic and Electronic Applications

Cholesterol-containing polymers, on top of their excellent biocompatibility, have shown promise as future materials in photonic and electronic applications. Table 1 summarises some of the recent developments within these fields.

**Table 1.** List of various cholesterol-containing polymers and their applications in photonic and electronic devices.

Polymer Type	Components	Synthesis Method	Application	References
Elastomers	Poly(methylsilylene), cholesterylcarbonate and a cross linker	Hydrosilylation	Lasing	[82–84]
Block copolymers	Photochromic spirooxazine and cholesterol mesogen	Free radical polymerisation	Data storage	[85–87]
Homopolymers and copolymers	Methacrylates bearing cholesterol pendant group and methyl methacrylate	Atom transfer radical polymerisation (ATRP)	Organic field-effect transistor (OFET)	[88,89]
Cross-linked copolymer	Polybenzoxazine functionalised with cholesterol	Ring-opening polymerisation	High-thermal conductivity and heat-resistance	[90–92]
Block-copolymers	Azobenzene and cholesteryl mesogens	Ring-opening polymerisation	Photo-optical switching	[93,94]
Block-copolymers	Polyoxyethylene and cholesterol methacrylate	Reversible addition–fragmentation chain transfer (RAFT) polymerisation	Energy storage	[95]
Homopolymers	Polyphenylallenes with various spacers between backbone and cholesterol mesogen	Coordination polymerisation	Fluorescent sensors	[96–99]

As discussed in the Introduction, cholesterol-based liquid crystal polymers are well-known for their chiral nematic phase. Figure 14 shows the colour shift observed for a cholesteric liquid crystal elastomer as a function of strain. The colour change was observed due to the change in pitch of the elastomer. This polymer was then used for a low-

threshold, mirrorless lasing [82] The lasing effect was observed after doping the elastomer network with a 4-(dicyanomethylene)-2-methyl-6-(4-dimethyl-amino styryl)-4-H-pyran (DCM), a well-known laser dye. It was shown that the laser line of narrow line width, approx. 3 Å, could be shifted by applying mechanical strain to the elastomer (Figure 14). Another potential application of chiral nematic-based cholesterol polymers is data storage. Hattori et al. demonstrated the controlled pitch change of an N\* film upon exposure to UV irradiation [85]. Ndaya et al. [93] prepared a series of responsive copolymers based on azobenzene and cholesterol mesogens, which displayed a reversible change in their selective reflection, from near IR to visible light, as a function of temperature. This allows these materials to be employed as photo-optical switches.

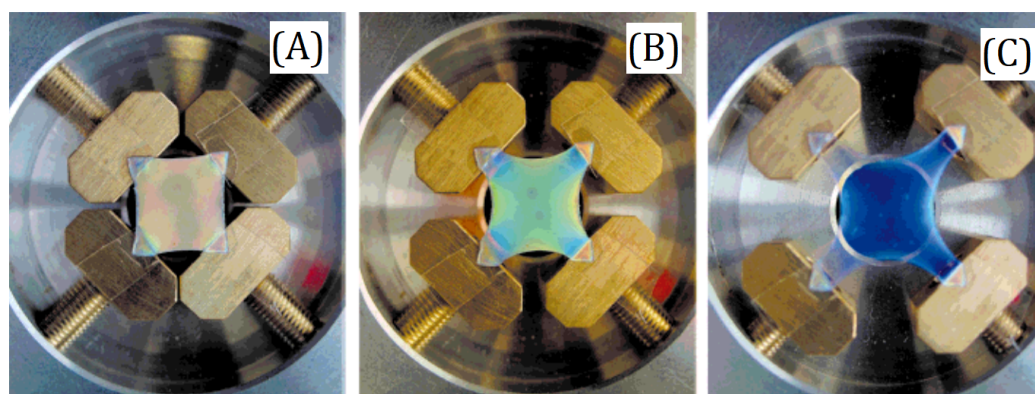


**Figure 14.** Colour shift observed for cholesteric liquid crystal elastomer as a function of strain. The colour change is observed due to change in the position of the reflection band of the elastomer as a function of mechanical deformation with unstrained sample (A) being green through to (B) light green, with blue in the corners, to strained sample (C), where the entire sample is blue. Reprinted with permission from Finkelmann et al., *Advanced Materials*, **2001**, *13*, 1069–1072.

Dognaci et al. [88] prepared a series of methacrylic homopolymers and copolymers bearing a cholesterol pendant group and methyl methacrylate. The Cole–Cole plot of most of the polymers prepared showed non-Debye relaxation behaviours, with the exception of two individual polymers. A homopolymer with a spacer length of 10 showed promise as a potential material for applications within organic photovoltaics, as it demonstrated DC conductivity behaviour at high frequencies.

A series of heat-resistant cross-linked polybenzoxazine-based polymers containing cholesterol mesogens was prepared by Liu et al. [90]. They demonstrated high thermal conductivity and showed thermal stability up to 300 °C, with a smectic range between 100 °C and 220 °C. Another potential application for a cholesterol-containing polymer is within solid-state energy storage and lithium ion batteries. Zhou et al. [95] prepared a series of copolymers of polyoxyethylene (PEO) and a methacrylic cholesteryl mesogen, which formed amorphous nanostructures of PEO at room temperature but maintained their mechanical properties at elevated temperatures. Shape memory polymers (SMPs) have a wide variety of applications, including within the field of photonics in the design of functional and responsive gratings. Mahajan et al. [100] studied SMP based on side chain cholesterol mesogens. They observed reversible shape transformation after stretching the polymer at elevated temperature and quenching to room temperature (Figure 15A–C). Ahn et al. [101] demonstrated the memory effect within terpolymer and explored it within the context of the smectic order director in relation to the long axis of the film formed (Figure 15D).

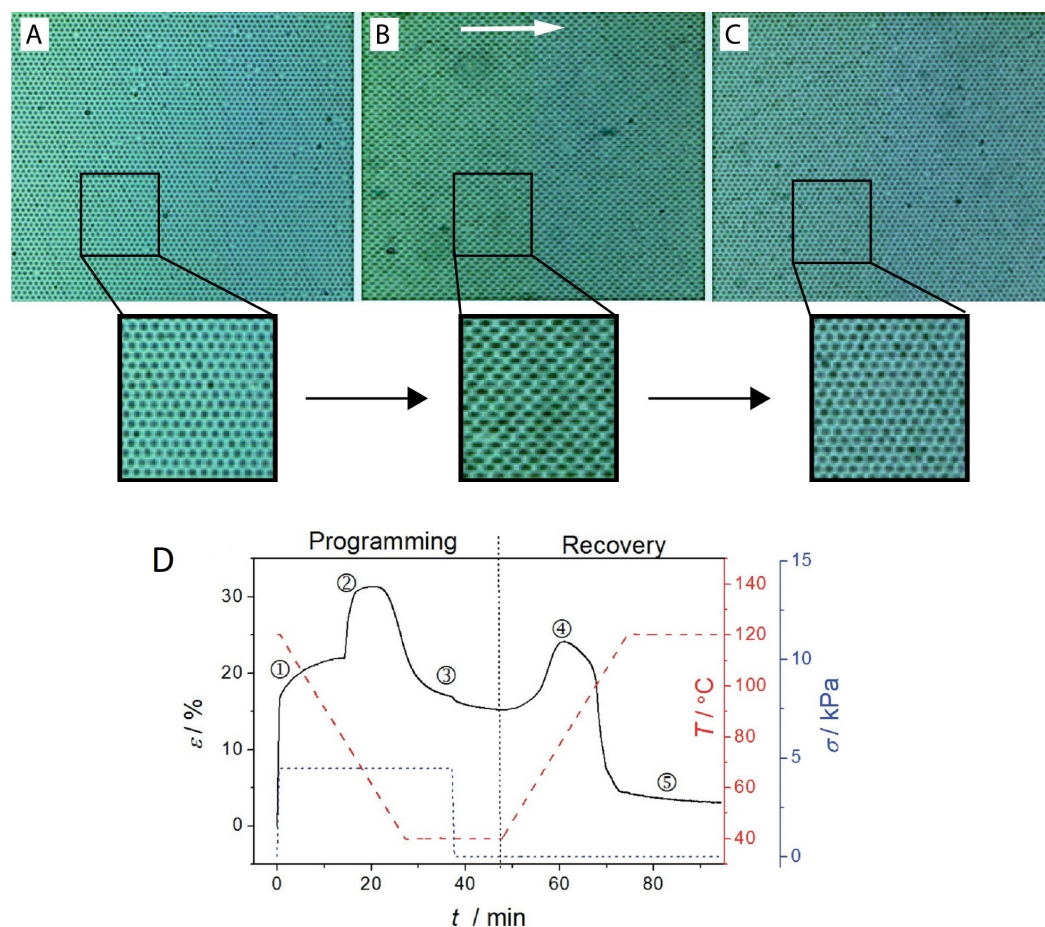


**Figure 15.** Shape memory effect (SMP) displayed by a cholesteric terpolymer film (A) stretched at 110 °C (B) quenched to room temperature and (C) recovering its original shape upon reheating back to 110 °C. (D) Shape memory effect of a film of a terpolymer and its subsequent recovery on heating shown as function of time. Red dashed line represents the response as a function of temperature, blue dotted line shows the strain applied and solid black line the strain response. Numbers 1 and 5 correspond to different isotropic states and 2 to 4 correspond to various SmA polymorphism change during shape memory effect. Reprinted with permission from Mahajan et al., *Macromolecules*, 2017, **50**, 5929–5939 and Ahn et al., *ACS Nano*, 2011, **5**, 3085–3095 [100,101].

As mentioned in Section 3.1.2, cholesterol-containing polymers can be made to display aggregation-induced emission (AIE) behaviour, which can act as a fluorescent probe. Zhang et al. [96] showed that a series of hydrogen-bonding polymers, depending on the linker between the backbone and cholesteryl mesogen, displayed both aggregation-induced emission and aggregation-induced quenching (AIQ).

#### 4. Conclusions and Outlook

Steroid-based liquid crystal polymers and co-polymers is a rapidly developing area of research with applications in a variety of fields. There are few reviews available on the topic of steroid-based polymers discussing the relevant chemical aspects and self-assembly capabilities [69,102–104]. In this review, cholesterol and related sterol-based polymers are described and their structure–property relationship is discussed, with particular emphasis on their liquid crystalline properties and their potential benefit in applications. These underlying principles, in combination with sterols' natural biocompatibility, make them excellent materials for use in drug delivery devices for anticancer, antimicrobial and anti-inflammatory drugs, as well as for imaging dyes. Their responsiveness has been utilised for controlled payload release in vivo with mammalian cells and in vitro. Their intrinsic

liquid crystalline behaviour has demonstrated a positive impact on artificial tissue growth. Applications of LC cholesterol-based elastomers within biomedicine as scaffolds for tissue growth have only recently been explored, but show tremendous promise due to low cytotoxicity and good biocompatibility. This is a feature not commonly found in standard liquid crystalline polymers, which makes the cholesterol-based polymers more relevant as materials of the future.

The versatile self-assembly behaviour and responsiveness to changes in the system, including solvent exposure, light and temperature, make steroid-based liquid crystal polymers and copolymers prime candidates for sensing and imaging applications. Their uniform, 1D structures have been shown to adapt, making them suitable for applications within nanoelectronics as charge carriers for micro- and nano-sized devices. Their liquid crystalline properties allow them to self-assemble into stable structures otherwise unavailable with non liquid crystalline blocks. Future directions of research in this area promise novel medical and technological developments. Further expanding and optimising the array of biocompatible polymers with cholesterol is being explored, particularly the potential applications in artificial tissue growth, not just for medical applications but also for lab-grown meat. The materials are being further developed for applications in the next generation of photovoltaics and fuel cells. The natural abundance of cholesterol and their ease of acquisition makes them suitable for scaling up on an industrial scale for the fabrication of such devices.

**Funding:** This research received no external funding.

**Institutional Review Board Statement:** Not applicable.

**Informed Consent Statement:** Not applicable.

**Data Availability Statement:** Not applicable.

**Conflicts of Interest:** The authors declare no conflict of interest.

## References

1. Reinitzer, F. Contributions to the knowledge of cholesterol. *Liq. Cryst.* **1989**, *5*, 7–18. [[CrossRef](#)]
2. Bullard, B.; Stumpf, C.H.; Zhao, W.; Kuzenko, S.; Niehaus, G.D. Crystal Diagnostics Xpress S Kit for the rapid detection of *Salmonella* spp. in selected food matrixes. *J. AOAC Int.* **2017**, *100*, 1038–1050. [[CrossRef](#)] [[PubMed](#)]
3. Schadt, M.; Helfrich, W. Voltage-dependent optical activity of a twisted nematic liquid crystal. *Appl. Phys. Lett.* **1971**, *18*, 127–128. [[CrossRef](#)]
4. Chang, C.; Bang, K.; Wetzstein, G.; Lee, B.; Gao, L. Toward the next-generation VR/AR optics: A review of holographic near-eye displays from a human-centric perspective. *Optica* **2020**, *7*, 1563. [[CrossRef](#)]
5. Milton, H.E.; Morgan, P.B.; Clamp, J.H.; Gleeson, H.F. Electronic liquid crystal contact lenses for the correction of presbyopia. *Opt. Express* **2014**, *22*, 8035. [[CrossRef](#)]
6. Heilmeyer, G.H.; Zanoni, L.A.; Barton, L.A. Dynamic scattering in nematic liquid crystals. *Appl. Phys. Lett.* **1968**, *13*, 46–47. [[CrossRef](#)]
7. Kowrdziej, R.; Garbat, K.; Walczakowski, M. Nematic liquid crystal mixtures dedicated to thermally tunable terahertz devices. *Liq. Cryst.* **2018**, *45*, 1040–1046. [[CrossRef](#)]
8. Caputo, R.; Palermo, G.; Infusino, M.; De Sio, L. Liquid Crystals as an Active Medium: Novel Possibilities in Plasmonics. *Nanospectroscopy* **2015**, *1*, 40–53. [[CrossRef](#)]
9. Wang, Z.; Xu, T.; Noel, A.; Chen, Y.C.; Liu, T. Applications of liquid crystals in biosensing. *Soft Matter* **2021**, *17*, 4675–4702. [[CrossRef](#)]
10. Hata, Y.; Insull, W. Significance of Cholesterol Esters as Liquid Crystal in Human Atherosclerosis. *Jpn. Circ. J.* **1973**, *37*, 269–275. [[CrossRef](#)]
11. Edward Barrall, b.M.; Porter, R.S.; Johnson, J.F.; Barrall, E.M.; Porter, R.S.; Johnson, J.F.; Phys, J.; Martin, H.; Müller, F.H. Molecular Structure and the Properties of Liquid Crystals. *Z. Physik Chem.* **1964**, *68*, 51.
12. Usoltseva, V.A.; Chistyakov, I.G. Chemical characteristics, structure, and properties of liquid crystal. *Russ. Chem. Rev.* **1963**, *32*, 495–509. [[CrossRef](#)]
13. Barrall, E.M.; Porter, R.S.; Johnson, J.F.; S Andrews, J.T. Heats of Transition for Some Cholesteryl Esters by Differential Scanning Calorimetry. *J. Phys. Chem.* **1967**, *71*, 1224–1228. [[CrossRef](#)]
14. Baessler, H.; Labes, M.M. Helical twisting power of steroidal solutes in cholesteric mesophases. *J. Chem. Phys.* **1970**, *52*, 631–637. [[CrossRef](#)] [[PubMed](#)]

15. Yu, X.H.; Zhang, D.W.; Zheng, X.L.; Tang, C.K. Cholesterol transport system: An integrated cholesterol transport model involved in atherosclerosis. *Prog. Lipid Res.* **2019**, *73*, 65–91. [[CrossRef](#)] [[PubMed](#)]
16. Thakur, V.K.; Kessler, M.R. *Liquid Crystalline Polymers*, 1st ed.; Springer International Publishing: Cham, Switzerland, 2016. [[CrossRef](#)]
17. Wang, X.J.; Zhou, Q.F. *Liquid Crystalline Polymers*; World Scientific: Singapur, 2004. [[CrossRef](#)]
18. Donald, A.M.; Windle, A.H.; Hanna, S. *Liquid Crystalline Polymers*; Cambridge University Press: Cambridge, UK, 2006. [[CrossRef](#)]
19. Wen, Z.; Yang, K.; Raquez, J.M. A review on liquid crystal polymers in free-standing reversible shape memory materials. *Molecules* **2020**, *25*, 1241. [[CrossRef](#)]
20. Trimmel, G.; Riegler, S.; Fuchs, G.; Slugovc, C.; Stelzer, F. Liquid Crystalline Polymers by Metathesis Polymerization. In *Metathesis Polymerization*; Buchmeiser, M.R., Ed.; Springer: Berlin/Heidelberg, Germany, 2005; pp. 43–87. [[CrossRef](#)]
21. Lyu, X.; Xiao, A.; Shi, D.; Li, Y.; Shen, Z.; Chen, E.Q.; Zheng, S.; Fan, X.H.; Zhou, Q.F. Liquid crystalline polymers: Discovery, development, and the future. *Polymer* **2020**, *202*, 122740. [[CrossRef](#)]
22. Platé, N.A.; Shibaev, V.P. Thermotropic liquid crystalline polymers—problems and trends. *Die Makromol. Chem.* **1984**, *6*, 3–27. [[CrossRef](#)]
23. Xie, Y.; Hu, J.; Dou, Q.; Xiao, L.; Yang, L. Synthesis and mesomorphism of new aliphatic polycarbonates containing side cholesteryl groups. *Liq. Cryst.* **2016**, *43*, 1486–1494. [[CrossRef](#)]
24. Doganci, E.; Davarci, D. Synthesized and mesomorphic properties of cholesterol end-capped poly( $\epsilon$ -caprolactone) polymers. *J. Polym. Res.* **2019**, *26*, 1–10. [[CrossRef](#)]
25. Finkelmann, H.; Ringsdorf, H.; Sol, W.; Wendolf, J.H. Synthesis of Cholesteric Liquid Crystalline Polymers Polyreactions in Ordered Systems, 15). *Makromol. Chem* **1978**, *179*, 829–832. [[CrossRef](#)]
26. Hessel, F.; Herr, R.P.; Finkelmann, H. Synthesis and characterization of biaxial nematic side chain polymers with laterally attached mesogenic groups. *Makromol. Chem* **1987**, *188*, 1597–1611. [[CrossRef](#)]
27. Shibaev, V.P.; Plate, N.A.; Freidzon, Y.S. Thermotropic Liquid Crystalline Polymers. I. Cholesterol-Containing Polymers and Copolymers. *J. Polym. Sci. Polym. Chem. Ed.* **1979**, *17*, 1655–670. [[CrossRef](#)]
28. Xu, X.; Liu, X.; Li, Q.; Hu, J.; Chen, Q.; Yang, L.; Lu, Y. New amphiphilic polycarbonates with side functionalized cholesteryl groups as biomesogenic units: Synthesis, structure and liquid crystal behavior. *RSC Adv.* **2017**, *7*, 14176–14185. [[CrossRef](#)]
29. Cowie, J.M.G.; Arrighi, V. *Polymers: Chemistry and Physics of Modern Materials*, 3rd ed.; CRC Press: Boca Raton, FL, USA, 2007.
30. Boissé, S.; Rieger, J.; Di-Cicco, A.; Albouy, P.A.; Bui, C.; Li, M.H.; Charleux, B. Synthesis via RAFT of amphiphilic block copolymers with liquid-crystalline hydrophobic block and their self-assembly in water. *Macromolecules* **2009**, *42*, 8688–8696. [[CrossRef](#)]
31. Huang, Z.H.; Zhou, Y.Y.; Wang, Z.M.; Li, Y.; Zhang, W.; Zhou, N.C.; Zhang, Z.B.; Zhu, X.L. Recent advances of CuAAC click reaction in building cyclic polymer. *Chin. J. Polym. Sci.* **2017**, *35*, 317–341. [[CrossRef](#)]
32. Hamley, I.W.; Castelletto, V.; Parras, P.; Lu, Z.B.; Imrie, C.T.; Itoh, T. Ordering on multiple lengthscales in a series of side group liquid crystal block copolymers containing a cholesteryl-based mesogen. *Soft Matter* **2005**, *1*, 355–363. [[CrossRef](#)]
33. Xu, J.P.; Ji, J.; Chen, W.D.; Shen, J.C. Novel biomimetic surfactant: Synthesis and micellar characteristics. *Macromol. Biosci.* **2005**, *5*, 164–171. [[CrossRef](#)]
34. Yang, S.Y.; Kang, J.H.; Jeong, S.Y.; Choi, K.H.; Lee, S.; Shin, G.J. Influence of chemical structure on the optical properties of new side-chain polymers containing cholesterol. *Liq. Cryst.* **2014**, *41*, 1286–1292. [[CrossRef](#)]
35. Finkelmann, H.; Kock, H.J.; Rehage, G. Investigations on Liquid Crystalline Polysiloxanes 3a) Liquid Crystalline Elastomers—A New Type of Liquid. *Makromol. Chem. Rapid Commun.* **1981**, *2*, 317–322. [[CrossRef](#)]
36. Hu, J.S.; Zhang, B.Y.; Jia, Y.G.; Wang, Y. Structures and Properties of Side-Chain Cholesteric Liquid Crystalline Polyacrylates. *Polym. J.* **2003**, *35*, 160–166. [[CrossRef](#)]
37. Yang, X.; Chen, S.; Chen, S.; Xu, H. Influencing factors on liquid crystalline properties of cholesterol side-chain liquid crystalline polymers without spacer: Molecular weight and copolymerisation. *Liq. Cryst.* **2019**, *46*, 1827–1842. [[CrossRef](#)]
38. Klok, H.A.; Hwang, J.J.; Iyer, S.N.; Stupp, S.I. Cholesteryl-(L-lactic acid) building blocks for self-assembling biomaterials. *Macromolecules* **2002**, *35*, 746–759. [[CrossRef](#)]
39. Wang, Y.; Zhang, B.Y.; He, X.Z.; Wang, J.W. Side-chain cholesteric liquid crystalline polymers containing menthol and cholesterol—Synthesis and characterization. *Colloid Polym. Sci.* **2007**, *285*, 1077–1084. [[CrossRef](#)]
40. Venkataraman, S.; Lee, A.L.; Maune, H.T.; Hedrick, J.L.; Prabhu, V.M.; Yang, Y.Y. Formation of disk- and stacked-disk-like self-assembled morphologies from cholesterol-functionalized amphiphilic polycarbonate diblock copolymers. *Macromolecules* **2013**, *46*, 4839–4846. [[CrossRef](#)]
41. Guo, Z.H.; Liu, X.F.; Hu, J.S.; Yang, L.Q.; Chen, Z.P. Synthesis and self-assembled behavior of pH-responsive chiral liquid crystal amphiphilic copolymers based on diosgenyl-functionalized aliphatic polycarbonate. *Nanomaterials* **2017**, *7*, 169. [[CrossRef](#)]
42. Li, L.; Zhou, F.; Li, Y.; Chen, X.; Zhang, Z.; Zhou, N.; Zhu, X. Cooperation of Amphiphilicity and Smectic Order in Regulating the Self-Assembly of Cholesterol-Functionalized Brush-Like Block Copolymers. *Langmuir* **2018**, *34*, 11034–11041. [[CrossRef](#)]
43. Krishnasamy, V.; Qu, W.; Chen, C.; Huo, H.; Ramanagul, K.; Gothandapani, V.; Mehl, G.H.; Mehl, G.H.; Zhang, Q.; Liu, F. Self-Assembly and Temperature-Driven Chirality Inversion of Cholesteryl-Based Block Copolymers. *Macromolecules* **2020**, *53*, 4193–4203. [[CrossRef](#)]
44. Hembury, G.A.; Borovkov, V.V.; Inoue, Y. Chirality-sensing supramolecular systems. *Chem. Rev.* **2008**, *108*, 1–73. [[CrossRef](#)]
45. Aviram, A.; Ratner, M.A. Molecular rectifiers. *Chem. Phys. Lett.* **1974**, *29*, 277–283. [[CrossRef](#)]

46. Morgenstern, K. Switching individual molecules by light and electrons: From isomerisation to chirality flip. *Prog. Surf. Sci.* **2011**, *86*, 115–161. [[CrossRef](#)]
47. Yang, H.; Jia, L.; Zhu, C.; Di-Cicco, A.; Levy, D.; Albouy, P.A.; Li, M.H.; Keller, P. Amphiphilic poly(ethylene oxide)-block-poly(butadiene-graft-liquid crystal) copolymers: Synthesis and self-assembly in water. *Macromolecules* **2010**, *43*, 10442–10451. [[CrossRef](#)]
48. Jia, L.; Cao, A.; Lévy, D.; Xu, B.; Albouy, P.A.; Xing, X.; Bowick, M.J.; Li, M.H. Smectic polymer vesicles. *Soft Matter* **2009**, *5*, 3446–3451. [[CrossRef](#)]
49. Jones, R.A. Challenges in soft nanotechnology. *Faraday Discuss.* **2009**, *143*, 9–14. [[CrossRef](#)] [[PubMed](#)]
50. Zhou, L.; Zhang, D.; Hocine, S.; Pilone, A.; Trépout, S.; Marco, S.; Thomas, C.; Guo, J.; Li, M.H. Transition from smectic nanofibers to smectic vesicles in the self-assemblies of PEG-*b*-liquid crystal polycarbonates. *Polym. Chem.* **2017**, *8*, 4776–4780. [[CrossRef](#)]
51. Jia, L.; Liu, M.; Di Cicco, A.; Albouy, P.A.; Brissault, B.; Penelle, J.; Boileau, S.; Barbier, V.; Li, M.H. Self-assembly of amphiphilic liquid crystal polymers obtained from a cyclopropane-1,1-dicarboxylate bearing a cholesteryl mesogen. *Langmuir* **2012**, *28*, 11215–11224. [[CrossRef](#)]
52. Jeong, Y.H.; Ahn, T.; Yu, W.; Lee, S.M. Cholesterol-Functionalized Linear/Brush Block Copolymers for Metal-Incorporated Nanostructures with Modulated Core Density and Enhanced Self-Assembly Efficiency. *ACS Macro Lett.* **2021**, *10*, 492–497. [[CrossRef](#)]
53. Jia, L.; Albouy, P.A.; Di Cicco, A.; Cao, A.; Li, M.H. Self-assembly of amphiphilic liquid crystal block copolymers containing a cholesteryl mesogen: Effects of block ratio and solvent. *Polymer* **2011**, *52*, 2565–2575. [[CrossRef](#)]
54. Zhang, X.; Boissé, S.; Bui, C.; Albouy, P.A.; Brûlet, A.; Li, M.H.; Rieger, J.; Charleux, B. Amphiphilic liquid-crystal block copolymer nanofibers via RAFT-mediated dispersion polymerization. *Soft Matter* **2012**, *8*, 1130–1141. [[CrossRef](#)]
55. Huo, M.; Zhang, Y.; Zeng, M.; Liu, L.; Wei, Y.; Yuan, J. Morphology Evolution of Polymeric Assemblies Regulated with Fluoro-Containing Mesogen in Polymerization-Induced Self-Assembly. *Macromolecules* **2017**, *50*, 8192–8201. [[CrossRef](#)]
56. Li, Y.; Lu, Q.; Chen, Q.; Wu, X.; Shen, J.; Shen, L. Directional effect on the fusion of ellipsoidal morphologies into nanorods and nanotubes. *RSC Adv.* **2021**, *11*, 1729–1735. [[CrossRef](#)] [[PubMed](#)]
57. Huo, M.; Song, G.; Zhang, J.; Wei, Y.; Yuan, J. Nonspherical Liquid Crystalline Assemblies with Programmable Shape Transformation. *ACS Macro Lett.* **2018**, *7*, 956–961. [[CrossRef](#)] [[PubMed](#)]
58. Huo, M.; Li, D.; Song, G.; Zhang, J.; Wu, D.; Wei, Y.; Yuan, J. Semi-Fluorinated Methacrylates: A Class of Versatile Monomers for Polymerization-Induced Self-Assembly. *Macromol. Rapid Commun.* **2018**, *39*, 1700840–1700846. [[CrossRef](#)] [[PubMed](#)]
59. Shen, L.; Guo, H.; Zheng, J.; Wang, X.; Yang, Y.; An, Z. RAFT Polymerization-Induced Self-Assembly as a Strategy for Versatile Synthesis of Semifluorinated Liquid-Crystalline Block Copolymer Nanoobjects. *ACS Macro Lett.* **2018**, *7*, 287–292. [[CrossRef](#)] [[PubMed](#)]
60. Li, X.; Jin, B.; Gao, Y.; Hayward, D.W.; Winnik, M.A.; Luo, Y.; Manners, I. Monodisperse Cylindrical Micelles of Controlled Length with a Liquid-Crystalline Perfluorinated Core by 1D “Self-Seeding”. *Angew. Chem.* **2016**, *128*, 11564–11568. [[CrossRef](#)]
61. Guan, S.; Chen, A. Influence of Spacer Lengths on the Morphology of Biphenyl-Containing Liquid Crystalline Block Copolymer Nanoparticles via Polymerization-Induced Self-Assembly. *Macromolecules* **2020**, *53*, 6235–6245. [[CrossRef](#)]
62. Guan, S.; Zhang, C.; Wen, W.; Qu, T.; Zheng, X.; Zhao, Y.; Chen, A. Formation of Anisotropic Liquid Crystalline Nanoparticles via Polymerization-Induced Hierarchical Self-Assembly. *ACS Macro Lett.* **2018**, *7*, 358–363. [[CrossRef](#)]
63. Wen, W.; Ouyang, W.; Guan, S.; Chen, A. Synthesis of azobenzene-containing liquid crystalline block copolymer nanoparticles: Via polymerization induced hierarchical self-assembly. *Polym. Chem.* **2021**, *12*, 458–465. [[CrossRef](#)]
64. Wen, W.; Chen, A. The self-assembly of single chain Janus nanoparticles from azobenzene-containing block copolymers and reversible photoinduced morphology transitions. *Polym. Chem.* **2021**, *12*, 2447–2456. [[CrossRef](#)]
65. Zhang, N.; Fan, Y.; Chen, H.; Trépout, S.; Brûlet, A.; Li, M.H. Polymersomes with a smectic liquid crystal structure and AIE fluorescence. *Polym. Chem.* **2022**, *13*, 1107–1115. [[CrossRef](#)]
66. Derry, M.J.; Fielding, L.A.; Warren, N.J.; Mable, C.J.; Smith, A.J.; Mykhaylyk, O.O.; Armes, S.P. In situ small-angle X-ray scattering studies of sterically-stabilized diblock copolymer nanoparticles formed during polymerization-induced self-assembly in non-polar media. *Chem. Sci.* **2016**, *7*, 5078–5090. [[CrossRef](#)]
67. Warren, N.J.; Mykhaylyk, O.O.; Ryan, A.J.; Williams, M.; Doussineau, T.; Dugourd, P.; Antoine, R.; Portale, G.; Armes, S.P. Testing the vesicular morphology to destruction: Birth and death of diblock copolymer vesicles prepared via polymerization-induced self-assembly. *J. Am. Chem. Soc.* **2015**, *137*, 1929–1937. [[CrossRef](#)] [[PubMed](#)]
68. Wang, S.; Luo, Y.; Li, X. Liquid crystal block copolymer micelles with aggregation-induced emission from corona chains. *J. Phys. Conf. Ser.* **2020**, *1605*, 012173. [[CrossRef](#)]
69. Albuquerque, H.M.; Santos, C.M.; Silva, A.M. Cholesterol-based compounds: Recent advances in synthesis and applications. *Molecules* **2019**, *24*, 116. [[CrossRef](#)] [[PubMed](#)]
70. Hwang, J.J.; Iyer, S.N.; Li, L.S.; Claussen, R.; Harrington, D.A.; Stupp, S.I. Self-assembling biomaterials: Liquid crystal phases of cholesteryl oligo(L-lactic acid) and their interactions with cells. *Proc. Natl. Acad. Sci. USA* **2002**, *99*, 9662–9667. [[CrossRef](#)]
71. Prévôt, M.E.; Andro, H.; Alexander, S.L.; Ustunel, S.; Zhu, C.; Nikolov, Z.; Rafferty, S.T.; Brannum, M.T.; Kinsel, B.; Korley, L.T.; et al. Liquid crystal elastomer foams with elastic properties specifically engineered as biodegradable brain tissue scaffolds. *Soft Matter* **2018**, *14*, 354–360. [[CrossRef](#)]

72. Xie, W.; Ouyang, R.; Wang, H.; Li, N.; Zhou, C. Synthesis and cytotoxicity of novel elastomers based on cholesteric liquid crystals. *Liq. Cryst.* **2020**, *47*, 449–464. [[CrossRef](#)]
73. Sharma, A.; Neshat, A.; Mahnen, C.J.; Nielsen, A.D.; Snyder, J.; Stankovich, T.L.; Daum, B.G.; Laspina, E.M.; Beltrano, G.; Gao, Y.; et al. Biocompatible, biodegradable and porous liquid crystal elastomer scaffolds for spatial cell cultures. *Macromol. Biosci.* **2015**, *15*, 200–214. [[CrossRef](#)]
74. Liu, Y.; Wang, Y.; Zhuang, D.; Yang, J.; Yang, J. Bionanoparticles of amphiphilic copolymers polyacrylate bearing cholesterol and ascorbate for drug delivery. *J. Colloid Interface Sci.* **2012**, *377*, 197–206. [[CrossRef](#)]
75. Lee, A.L.; Venkataraman, S.; Sirat, S.B.; Gao, S.; Hedrick, J.L.; Yang, Y.Y. The use of cholesterol-containing biodegradable block copolymers to exploit hydrophobic interactions for the delivery of anticancer drugs. *Biomaterials* **2012**, *33*, 1921–1928. [[CrossRef](#)]
76. Jia, L.; Cui, D.; Bignon, J.; Di Cicco, A.; Wdzieczak-Bakala, J.; Liu, J.; Li, M.H. Reduction-responsive cholesterol-based block copolymer vesicles for drug delivery. *Biomacromolecules* **2014**, *15*, 2206–2217. [[CrossRef](#)] [[PubMed](#)]
77. Liu, X.; Guo, Z.; Xie, Y.; Chen, Z.; Hu, J.; Yang, L. Synthesis and liquid crystal behavior of new side chain aliphatic polycarbonates based on cholesterol. *J. Mol. Liq.* **2018**, *259*, 350–358. [[CrossRef](#)]
78. Geihe, E.I.; Cooley, C.B.; Simon, J.R.; Kiesewetter, M.K.; Edward, J.A.; Hickerson, R.P.; Kaspar, R.L.; Hedrick, J.L.; Waymouth, R.M.; Wender, P.A.; et al. Designed guanidinium-rich amphiphathic oligocarbonate molecular transporters complex, deliver and release siRNA in cells. *Proc. Natl. Acad. Sci. USA* **2012**, *109*, 13171–13176. [[CrossRef](#)] [[PubMed](#)]
79. Liu, X.; Xie, Y.; Hu, Z.; Chen, Z.; Hu, J.; Yang, L. pH responsive self-assembly and drug release behavior of aliphatic liquid crystal block polycarbonate with pendant cholesteryl groups. *J. Mol. Liq.* **2018**, *266*, 405–412. [[CrossRef](#)]
80. Zhang, C.Y.; Xiong, D.; Sun, Y.; Zhao, B.; Lin, W.J.; Zhang, L.J. Self-assembled micelles based on pH-sensitive PAE-g-MPEG-cholesterol block copolymer for anticancer drug delivery. *Int. J. Nanomed.* **2014**, *9*, 4923–4933. [[CrossRef](#)] [[PubMed](#)]
81. Tran, T.H.; Nguyen, C.T.; Gonzalez-Fajardo, L.; Hargrove, D.; Song, D.; Deshmukh, P.; Mahajan, L.; Ndaya, D.; Lai, L.; Kasi, R.M.; et al. Long circulating self-assembled nanoparticles from cholesterol-containing brush-like block copolymers for improved drug delivery to tumors. *Biomacromolecules* **2014**, *15*, 4363–4375. [[CrossRef](#)] [[PubMed](#)]
82. Finkelmann, H.; Kim, S.T.; Muñoz, A.; Palffy-Muhoray, P.; Taheri, B. Tunable Mirrorless Lasing in Cholesteric Liquid Crystalline Elastomers. *Adv. Mater.* **2001**, *13*, 1069–1072. [[CrossRef](#)]
83. Kim, S.T.; Finkelmann, H. Cholesteric Liquid Single-Crystal Elastomers (LSCE) Obtained by the Anisotropic Deswelling Method. *Macromol. Rapid Commun* **2001**, *22*, 429–433. [[CrossRef](#)]
84. Varanytsia, A.; Nagai, H.; Urayama, K.; Palffy-Muhoray, P. Tunable lasing in cholesteric liquid crystal elastomers with accurate measurements of strain. *Sci. Rep.* **2015**, *5*, 1–8. [[CrossRef](#)]
85. Hattori, H.; Uryu, T. Synthesis and Properties of Photochromic Liquid-Crystalline Copolymers Containing Both Spiroanthoxazine and Cholesteryl Groups. *J. Polym. Sci. Part A Polym. Chem.* **2000**, *38*, 887–894. [[CrossRef](#)]
86. Petri, A.; Kummer, S.; Anneser, H.; Feiner, F.; Briiuchles, C. Photoinduced Reorientation of Cholesteric Liquid Crystalline Polysiloxanes Photoinduced Reorientation of Cholesteric Liquid Crystalline Polysiloxanes and Applications in Optical Information Storage and Second Harmonic Generation. *Berichte Bunsenges. Phys. Chem.* **1993**, *97*, 1281–1286. [[CrossRef](#)]
87. He, X.Z.; Gao, Y.F.; Zheng, J.J.; Li, X.Y.; Meng, F.B.; Hu, J.S. Chiral photosensitive side-chain liquid crystalline polymers—Synthesis and characterization. *Colloid Polym. Sci.* **2016**, *294*, 1823–1832. [[CrossRef](#)]
88. Doganci, E.; Cakirlar, C.; Bayir, S.; Yilmaz, F.; Yasin, M. Methacrylate based side chain liquid crystalline polymers with pendant cholesterol group: Preparation and investigation of electrical conductivity mechanism. *J. Appl. Polym. Sci.* **2017**, *134*, 45207. [[CrossRef](#)]
89. Doganci, E.; Kayabasi, F.; Davarçı, D.; Demir, A.; Gürek, A.G. Synthesis of liquid crystal polymers containing cholesterol side groups and investigation of their usability potential as an insulator in organic field effect transistor (OFET) applications. *J. Polym. Res.* **2022**, *29*, 147. [[CrossRef](#)]
90. Liu, Y.; Chen, J.; Qi, Y.; Gao, S.; Balaji, K.; Zhang, Y.; Xue, Q.; Lu, Z. Cross-linked liquid crystalline polybenzoxazines bearing cholesterol-based mesogen side groups. *Polymer* **2018**, *145*, 252–260. [[CrossRef](#)]
91. Suk-Kyun, A.H.; Le, L.T.; Kasi, R.M. Synthesis and characterization of side-chain liquid crystalline polymers bearing cholesterol mesogen. *J. Polym. Sci. Part A Polym. Chem.* **2009**, *47*, 2690–2701. [[CrossRef](#)]
92. Zhou, F.; Li, Y.; Jiang, G.; Zhang, Z.; Tu, Y.; Chen, X.; Zhou, N.; Zhu, X. Biomacrocyclic side-chain liquid crystalline polymers bearing cholesterol mesogens: Facile synthesis and topological effect study. *Polym. Chem.* **2015**, *6*, 6885–6893. [[CrossRef](#)]
93. Ndaya, D.; Bosire, R.; Kasi, R.M. Cholesteric-azobenzene liquid crystalline copolymers: Design, structure and thermally responsive optical properties. *Polym. Chem.* **2019**, *10*, 3868–3878. [[CrossRef](#)]
94. Ndaya, D.; Bosire, R.; Vaidya, S.; Kasi, R.M. Molecular engineering of stimuli-responsive, functional, side-chain liquid crystalline copolymers: Synthesis, properties and applications. *Polym. Chem.* **2020**, *11*, 5937–5954. [[CrossRef](#)]
95. Zhou, Y.; Ahn, S.K.; Lakhman, R.K.; Gopinadhan, M.; Osuji, C.O.; Kasi, R.M. Tailoring crystallization behavior of PEO-based liquid crystalline block copolymers through variation in liquid crystalline content. *Macromolecules* **2011**, *44*, 3924–3934. [[CrossRef](#)]
96. Zhang, X.J.; Gao, R.T.; Kang, S.M.; Wang, X.J.; Jiang, R.J.; Li, G.W.; Zhou, L.; Liu, N.; Wu, Z.Q. Hydrogen-bonding dependent nontraditional fluorescence polyphenylallenes: Controlled synthesis and aggregation-induced emission behaviors. *Polymer* **2022**, *245*. [[CrossRef](#)]

97. Luo, Z.W.; Tao, L.; Zhong, C.L.; Li, Z.X.; Lan, K.; Feng, Y.; Wang, P.; Xie, H.L. High-efficiency circularly polarized luminescence from chiral luminescent liquid crystalline polymers with aggregation-induced emission properties. *Macromolecules* **2020**, *53*, 9758–9768. [[CrossRef](#)]
98. Wu, Y.; You, L.H.; Yu, Z.Q.; Wang, J.H.; Meng, Z.; Liu, Y.; Li, X.S.; Fu, K.; Ren, X.K.; Tang, B.Z. Rational Design of Circularly Polarized Luminescent Aggregation-Induced Emission Luminogens (AIEgens): Promoting the Dissymmetry Factor and Emission Efficiency Synchronously. *ACS Mater. Lett.* **2020**, *2*, 505–510. [[CrossRef](#)]
99. Song, F.; Cheng, Y.; Liu, Q.; Qiu, Z.; Lam, J.W.; Lin, L.; Yang, F.; Tang, B.Z. Tunable circularly polarized luminescence from molecular assemblies of chiral AIEgens. *Mater. Chem. Front.* **2019**, *3*, 1768–1778. [[CrossRef](#)]
100. Mahajan, L.H.; Ndaya, D.; Deshmukh, P.; Peng, X.; Gopinadhan, M.; Osuji, C.O.; Kasi, R.M. Optically Active Elastomers from Liquid Crystalline Comb Copolymers with Dual Physical and Chemical Cross-Links. *Macromolecules* **2017**, *50*, 5929–5939. [[CrossRef](#)]
101. Ahn, S.K.; Deshmukh, P.; Gopinadhan, M.; Osuji, C.O.; Kasi, R.M. Side-chain liquid crystalline polymer networks: Exploiting nanoscale smectic polymorphism to design shape-memory polymers. *ACS Nano* **2011**, *5*, 3085–3095. [[CrossRef](#)]
102. Zhou, Y.; Briand, V.A.; Sharma, N.; Ahn, S.k.; Kasi, R.M. Polymers comprising cholesterol: Synthesis, self-assembly, and applications. *Materials* **2009**, *2*, 636–660. [[CrossRef](#)]
103. Hosta-Rigau, L.; Zhang, Y.; Teo, B.M.; Postma, A.; Städler, B. Cholesterol-A biological compound as a building block in bionanotechnology. *Nanoscale* **2013**, *5*, 89–109. [[CrossRef](#)]
104. Misiak, P.; Markiewicz, K.H.; Szymczuk, D.; Wilczewska, A.Z. Polymeric drug delivery systems bearing cholesterol moieties: A review. *Polymers* **2020**, *12*, 2620. [[CrossRef](#)]